

Substituents on the end group subtle tuning the energy levels and absorptions of small-molecule nonfullerene acceptors

Xin Ke, Bin Kan, Xiangjian Wan, Yunchuang Wang, Yamin Zhang, Chenxi Li, Yongsheng Chen*

State Key Laboratory and Institute of Elemento-Organic Chemistry, The Centre of Nanoscale Science and Technology and Key Laboratory of Functional Polymer Materials, College of Chemistry, Nankai University, Tianjin, 300071, China

ARTICLE INFO

Keywords:

End group
Small-molecule
Nonfullerene acceptor
Organic solar cell

ABSTRACT

Two new small-molecule nonfullerene acceptors containing methyl- and fluorine-substituted 2-(2,3-dihydro-3-oxo-1*H*-inden-1-ylidene)propanedinitrile (INCN) as end groups, namely, NFBDT-Me and NFBDT-F, were designed, synthesized and applied in organic solar cells. The influence of the methyl and fluorine groups on the absorption ability, energy levels, and photovoltaic performances was fully investigated. Compared to their parent molecule NFBDT, these two nonfullerene acceptors based devices exhibit higher PCEs with values of 11.00% and 10.62%, respectively. For NFBDT-Me, the improvement of PCE is mainly attributed to the higher V_{oc} , while for NFBDT-F, the increase of J_{sc} promotes the higher PCE. This suggests that appropriate manipulation of the end-group substituents of these non-fullerene acceptors is a promising way to enhance the PCEs of non-fullerene based OSCs.

1. Introduction

Organic solar cells (OSCs) are considered to be one of the green energy alternatives for future renewable energy conversion, because of their advantageous features such as light weight, flexibility and solution-based fabrication [1–3]. Due to the development of new donor materials and device optimization, the fullerene-based OSCs have achieved great success [4–9]. Presently, power conversion efficiencies (PCEs) over 11% have been achieved for OSCs with a bulk heterojunction (BHJ) architecture and fullerene derivatives as acceptors [10–15]. However, it is a great challenge for fullerene-based OSCs to achieve further improvements in photovoltaic performance owing to the disadvantages of fullerene derivatives, such as weak absorption, hardly changed energy levels and high cost synthesis and purification process [16,17]. To address these issues, numerous nonfullerene acceptor materials have been developed rapidly in recent years [11,18–26]. Zhan et al. reported some A-D-A type nonfullerene small-molecule acceptors using indacenothiophene (IDT) or indacenodithieno[3,2-b]thiophene (IDTT) as central building blocks, such as IDIC, ITIC and ITIC-Th [27–29]. Li et al. reported a nonfullerene acceptor *m*-ITIC with a PCE of 11.77% [24]. IT-4F reported by Hou et al. has a remarkable high PCE, which is over 13% [10]. Just recently, a nonfullerene acceptor based OSC with PCE over 14% have been reported by Ding et al. using near infrared absorption acceptor [30].

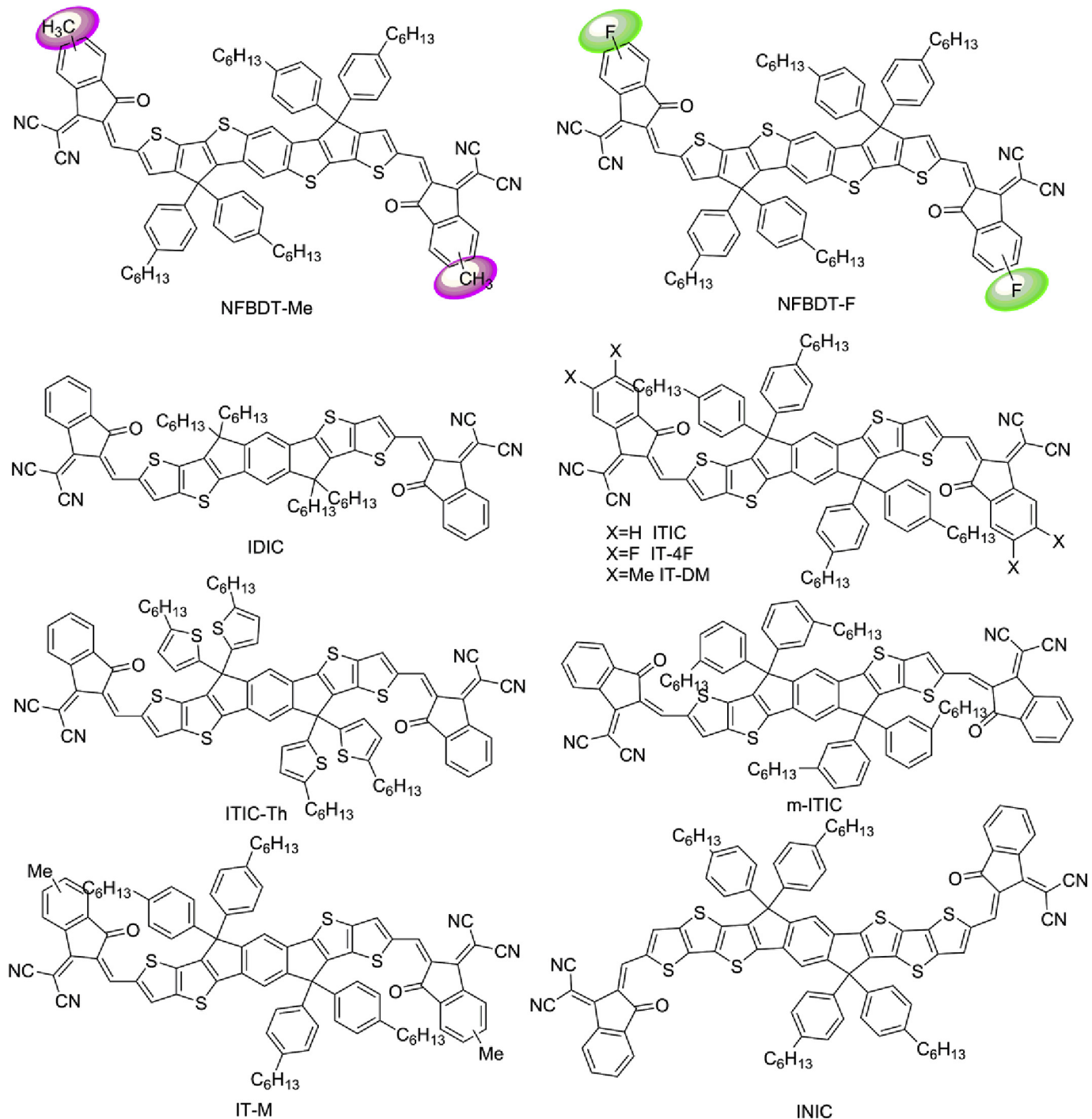
In order to obtain high-performance nonfullerene acceptors, many

design strategies have been explored [18,31–42]. Among these strategies, changing the substituents on the end group is an effective way to tune the energy levels and absorption, thus affecting their photovoltaic performance [10–12,19,43,44]. The methyl group is a weak electron-donating substituent, which can lift the LUMO levels without causing obvious steric hindrance. For example, Hou and his coworkers reported two nonfullerene acceptors, IT-M and IT-DM, which has one and two methyl substituents on the end group, respectively [11]. Compared with ITIC, the LUMO levels of IT-M and IT-DM are raised with values of 0.04 and 0.09 eV, respectively. Meanwhile, the fluorine has stronger electron-withdrawing ability and facilitates intermolecular interactions through forming F–S and F–H bonds [19]. Fluorination simultaneously down-shifts the highest occupied molecular orbital (HOMO) and the lowest unoccupied molecular orbital (LUMO) levels without causing strong steric hindrance of the resulting molecules [10,19,44–46]. For example, Zhan and his coworkers reported a serials of nonfullerene acceptors based on INIC [19]. The acceptors with fluorine substituents have lower LUMO level and narrower band gaps than that without fluorine substituent, which gives red-shifted absorptions and thus help to improve the J_{sc} and PCE.

Recently, a nonfullerene acceptor NFBDT, using heptacyclic benzodi(cyclopentadithiophene) (FBDT) as the core unit was reported and gave a PCE of 10.42% [47,48]. Herein, to investigate the influence of different substituents on the end group and further enhance the photovoltaic performance, we choose methyl and fluorine as the substituents

* Corresponding author.

E-mail address: yschen99@nankai.edu.cn (Y. Chen).



Scheme 1. The chemical structures of NFBDT-Me, NFBDT-F and some acceptors mentioned.

on the end group INCN, and designed two new nonfullerene acceptors, namely, NFBDT-Me and NFBDT-F. The chemical structures of NFBDT-Me and NFBDT-F together with some acceptors mentioned above are shown in Scheme 1. The influence of methyl and fluorine on the absorption ability, energy levels, and photovoltaic performances was fully investigated. The results demonstrate that a methyl group could indeed lift the LUMO levels and obtain higher V_{oc} for the devices while fluorine down-shift the LUMO levels and decreases the band gap, which makes the maximum absorption peak red-shift, thus increases the J_{sc} . With PBDB-T as donor, the devices based on NFBDT-Me and NFBDT-F gave a PCE of 11.00% and 10.62%, respectively. For NFBDT-Me based devices, the improvement of PCE is attributed to the higher V_{oc} and FF,

while for NFBDT-F based devices, the improvement is mainly attributed to the increase of J_{sc} .

2. Materials and methods

2.1. Materials

All reactions and manipulations were carried out under an argon atmosphere with the use of standard Schlenk techniques. Compound BDT, INCN-Me and INCN-F were purchased from corporation of Suzhou senior Bio. Compound FBBDT were synthesized according to the literature [49]. Other starting materials were purchased from

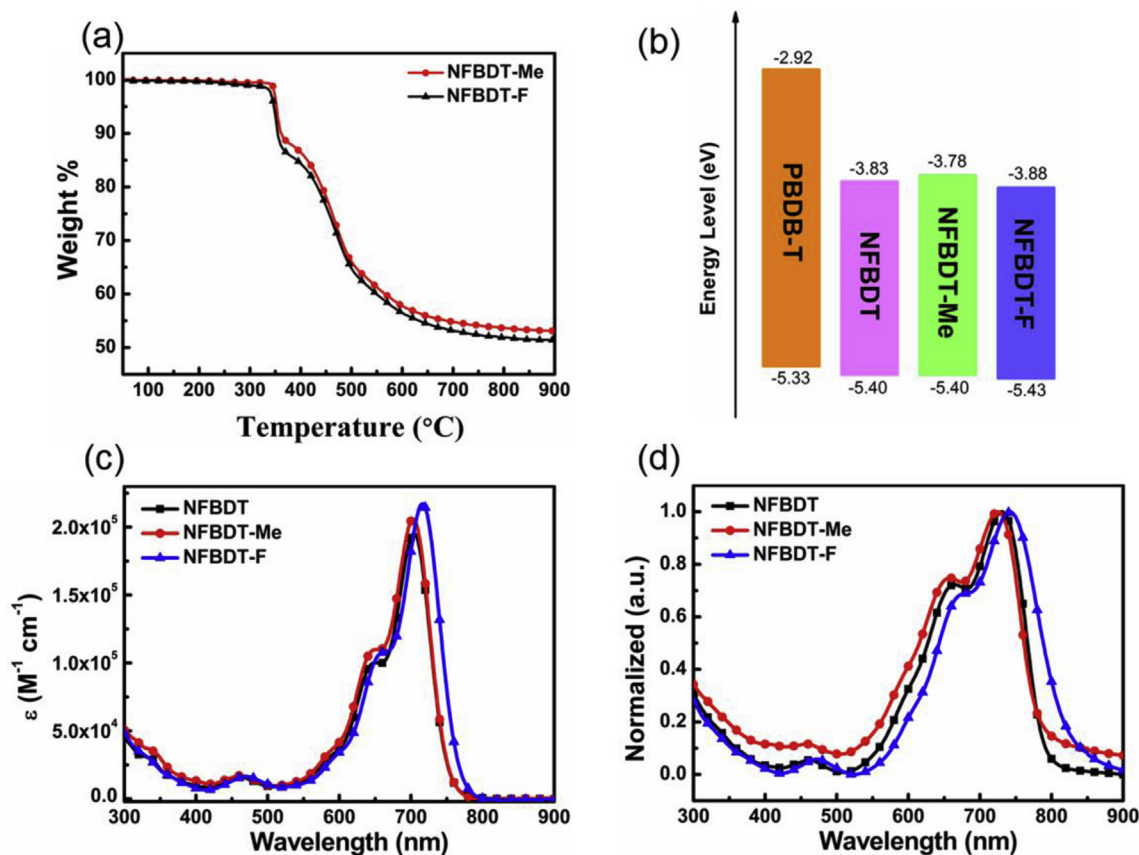


Fig. 1. (a) Thermogravimetric analysis (TGA) plot of NFBDT-Me and NFBDT-F with a heating rate of $10\text{ }^{\circ}\text{C min}^{-1}$ under N_2 atmosphere. (b) Energy levels of the donor and acceptors. (c) Absorption spectra of NFBDT-Me and NFBDT-F in CHCl_3 and (d) as film.

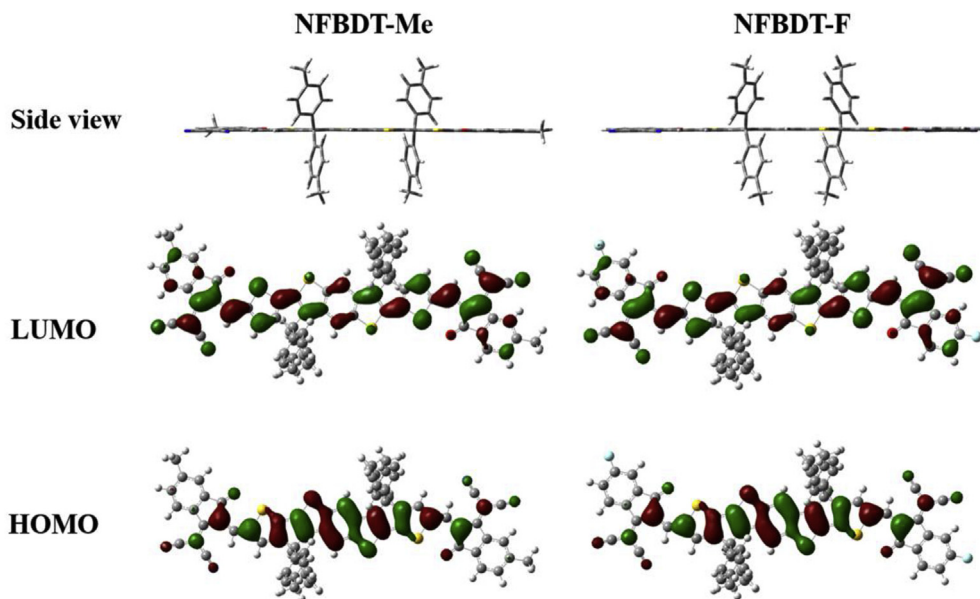


Fig. 2. The optimized geometries of NFBDT-Me and NFBDT-F using DFT calculations (B3LYP/6-31G(d)).

commercial suppliers and used without further purification unless otherwise noticed.

2.2. Instruments and measurements

The ^1H and ^{13}C NMR spectra were recorded on a Bruker AV400 Spectrometer. HRMS data were recorded on Varian 7.0T FT-MS. Fourier

Transform infrared spectroscopy (FTIR) was carried out using Bio-rad FTS-6000 FT-IR spectrometer. The thermogravimetric analysis (TGA) was carried out on a NETZSCH STA 449 F5 Jupiter instrument under purified nitrogen gas flow. The heating rate for TGA testing is $10\text{ }^{\circ}\text{C min}^{-1}$. UV-Vis spectra were obtained with a JASCO V-570 spectrophotometer.

Cyclic voltammetry (CV) experiments were performed with a

Table 1
Optical and electrochemical data of NFBDT-Me and NFBDT-F.

Molecules	$\lambda_{\text{max}}^{\text{soi}}$ (nm)	$\lambda_{\text{max}}^{\text{film}}$ (nm)	$\lambda_{\text{onset}}^{\text{film}}$ (nm)	E_g^{opt} (eV)	HOMO ^{CV} (eV)	LUMO ^{CV} (eV)	HOMO ^{Cal} (eV)	LUMO ^{Cal} (eV)
NFBDT-Me	702	725	786	1.58	-5.40	-3.78	-5.35	-3.29
NFBDT-F	717	743	826	1.50	-5.43	-3.88	-5.47	-3.44
NFBDT ^a	703	731	792	1.56	-5.40	-3.83	-5.40	-3.35

^a Data are obtained from Ref. [47].

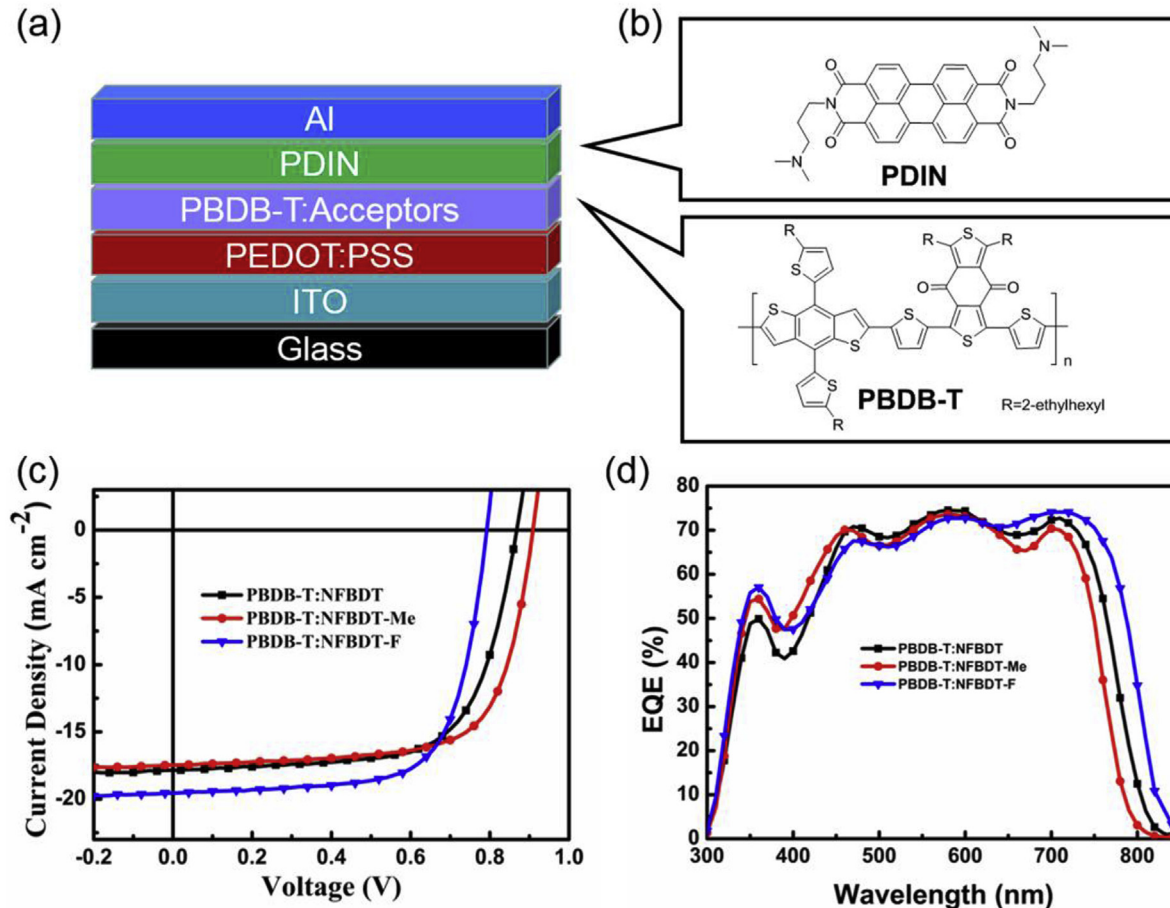


Fig. 3. (a) Device structure of the OSCs (b) Chemical structures of PDIN and PBDB-T (c) Current density – voltage (J – V) curves of the devices based on PBDB-T: Acceptors (d) EQE curves based on the devices.

Table 2

The photovoltaic performance of NFBDT-Me and NFBDT-F based devices.

Molecules	V_{oc} (V)	J_{sc} (mA cm^{-2})	$J_{\text{sc}}^{\text{EQE}}$ (mA cm^{-2})	FF	PCE(%) ^b
NFBDT-Me	0.909	17.30	16.70	70.0	11.00(10.82)
NFBDT-F	0.793	19.28	18.58	69.5	10.62(10.51)
NFBDT ^a	0.872	17.85	17.54	67.2	10.42(10.15)

^a Data are obtained from Ref. [47].

^b Average PCE values obtained from twenty devices are shown in parentheses.

LK2010 electrochemical workstation. All CV measurements were carried out at room temperature with a conventional three-electrode configuration employing a glassy carbon electrode as the working electrode, a saturated calomel electrode (SCE) as the reference electrode, and a Pt wire as the counter electrode. Dichloromethane was distilled from calcium hydride under dry nitrogen immediately prior to use. Tetrabutylammonium phosphorus hexafluoride (Bu_4NPF_6 , 0.1 M) in dry dichloromethane was used as the supporting electrolyte, and the

scan rate was 100 mV s^{-1} . The highest occupied molecular orbital (HOMO) and lowest unoccupied molecular orbital (LUMO) energy levels were calculated from the onset oxidation potential and the onset reduction potential, using the equation $E_{\text{HOMO}} = - (4.80 + E_{\text{onset}}^{\text{ox}})$, $E_{\text{LUMO}} = - (4.80 + E_{\text{onset}}^{\text{re}})$.

The geometry structures of NFBDT-Me and NFBDT-F were optimized by using DFT calculations (B3LYP/6-31G*), and the frequency analysis was followed to assure that the optimized structures were stable states. All calculations were carried out using Gaussian 09 [50].

Atomic force microscopy (AFM) investigation was performed using Bruker MultiMode 8 in tapping mode. The transmission electron microscopy (TEM) investigation was performed on Philips Technical G² F20 at 200 kV. The film samples for TEM measurement were prepared by spin casting the blend solution on ITO/PEDOT:PSS substrate, then were floated on a water surface, and transferred to TEM grids.

The hole and electron mobility were measured using the space charge limited current (SCLC) method, employing a diode configuration of ITO/PEDOT:PSS/active layer/Au for hole and glass/Al/active layer/Al for electron and fitting the results to a space charge limited form, where SCLC is described by:

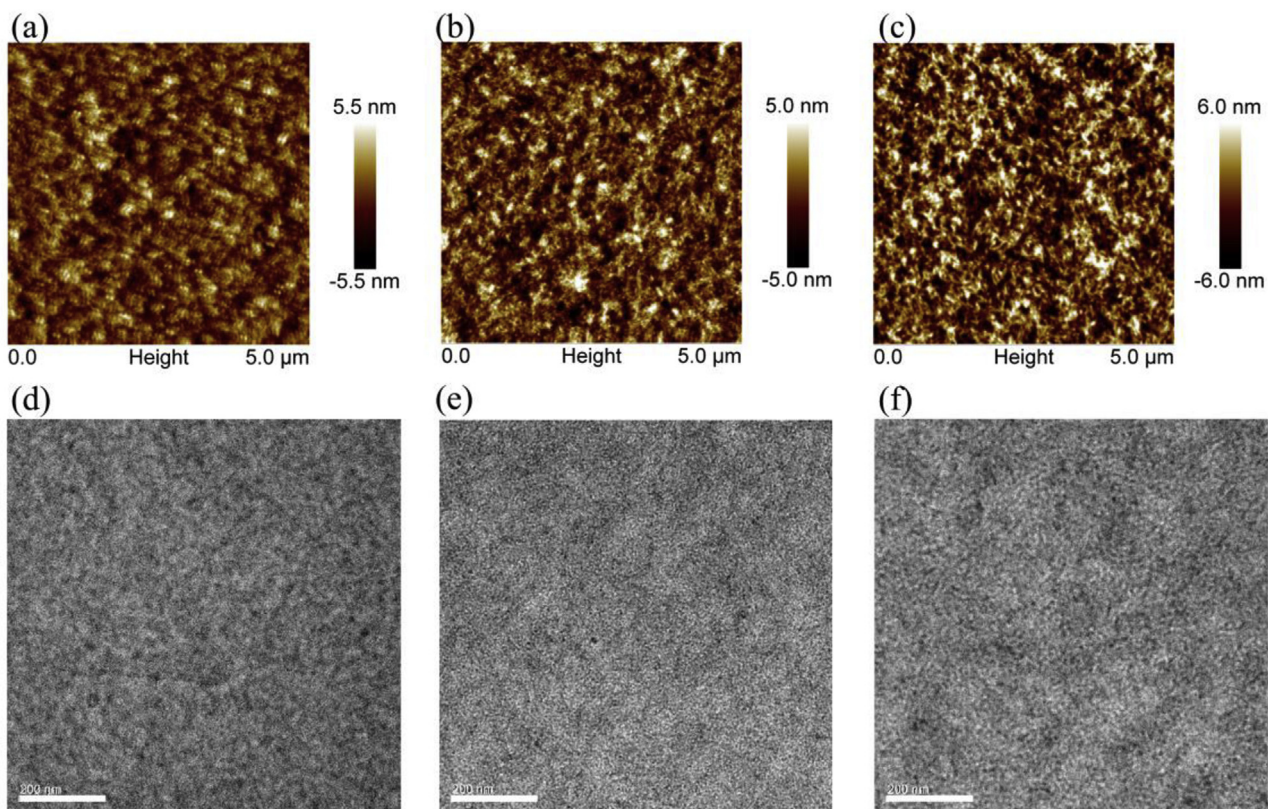


Fig. 4. Tapping-mode AFM image of the film (a) PBDB-T: NFBDT, (b) PBDB-T: NFBDT-Me, (c) PBDB-T: NFBDT-F, TEM images of the film (d) PBDB-T: NFBDT blend film, (e) PBDB-T: NFBDT-Me, (f) PBDB-T: NFBDT-F. The scale bars are 200 nm.

$$J = \frac{9\epsilon_0\epsilon_r\mu_0 V^2}{8L^3} \exp\left(0.89\beta\sqrt{\frac{V}{L}}\right)$$

where J is the current density, L is the film thickness of the active layer, μ is the hole or electron mobility, ϵ_r is the relative dielectric constant of the transport medium, ϵ_0 is the permittivity of free space ($8.85 \times 10^{-12} \text{ F m}^{-1}$), $V (= V_{\text{appl}} - V_{\text{bi}})$ is the internal voltage in the device, where V_{appl} is the applied voltage to the device and V_{bi} is the built-in voltage due to the relative work function difference of the two electrodes.

2.3. Solar cell fabrication and testing

The photovoltaic devices were fabricated with a structure of glass/ITO/PEDOT: PSS/Donor:Acceptor/PDIN/Al. The ITO-coated glass substrates were cleaned by detergent, deionized water, acetone, and isopropyl alcohol under ultrasonication for 15 min each and dried by a nitrogen blow. PEDOT: PSS layer was spin-coated (ca. 30 nm thick) onto the cleaned ITO surface. The substrates were then baked at 150 °C for 20 min. Subsequently, the active layer was spin-coated from donor and acceptor in chloroform solution at 1500 rpm for 20 s on the ITO/PEDOT: PSS substrate. The active layers were placed in a glass Petri dish for solvent vapor annealing. Then, PDIN (1.5 mg/mL using CH₃OH/AcOH (v: v = 100:0.2%) as mixed solvent) was spin-coated at 3000 rpm for 40 s on the active layer. Finally, a 60 nm Al layer were deposited on the PDIN layer under high vacuum (< 1.5 × 10⁻⁴ Pa). The effective area of each cell was 4 mm².

2.4. Synthesis

2.4.1. Synthesis of compound NFBDT-Me

Under the protection of argon, DCHOBDT (0.10 g, 0.093 mmol) and INCN-Me (0.077 g, 0.37 mmol) was dissolved in a dry CHCl₃

(50 mL) solution, and then pyridine (0.5 mL) was added to the mixture. After stirring at room temperature for 12 h, the mixture was poured into water and then extracted with CHCl₃ (30 mL × 2), the organic layer was dried over anhydrous Na₂SO₄ for 0.5 h. After removal of solvent, the crude product was purified by silica gel using petroleum ether/CHCl₃ (1:2) as eluent and recrystallized from CHCl₃ and hexane to give NFBDT-Me as a dark blue solid (0.107 g, 79.3% yield). Melting point: 214–217 °C. IR (KBr pellet): ν/cm^{-1} 2924.19, 2854.24, 2216.34, 1694.72, 1593.69, 1561.44, 1542.85, 1510.94, 1484.84, 1416.76, 1383.07, 1348.77, 1311.51, 1274.13, 1256.60, 1235.60, 1185.70, 1171.42, 1145.00, 1127.75, 991.71, 969.85, 878.11, 849.56, 655.24. ¹H NMR (400 MHz, CDCl₃): δ 8.83 (s, 2H), 8.53 (d, J = 8.1 Hz, 0.86H), 8.46 (s, 1.14H), 8.01 (s, 2H), 7.78 (d, J = 7.7 Hz, 1.14H), 7.68 (s, 2.86H), 7.53–7.50 (m, 2H), 7.15 (d, J = 8.2 Hz, 8H), 7.11 (d, J = 8.3 Hz, 8H), 2.55 (t, J = 7.7 Hz, 8H), 2.53 (s, 6H), 1.59–1.56 (m, 8H), 1.30–1.25 (m, 24H), 0.87–0.84 (m, 12H). ¹³C NMR (100 MHz, CDCl₃): δ 188.53, 188.18, 162.76, 160.22, 160.15, 155.81, 155.03, 154.86, 146.71, 146.18, 143.97, 142.63, 140.58, 140.32, 138.80, 138.76, 137.95, 137.76, 137.56, 137.42, 137.14, 135.37, 134.66, 131.75, 128.94, 128.85, 128.06, 125.63, 123.98, 123.56, 122.18, 122.13, 118.11, 114.88, 114.81, 68.53, 62.78, 35.61, 31.74, 31.65, 31.32, 29.76, 29.17, 26.97, 22.72, 22.65, 22.55, 22.05, 14.16. HR-MS (MALDI): Found: [M + H]⁺ 1455.5710 molecular formula C₉₆H₈₆N₄O₂S₄ requires [M + H]⁺, 1455.5712.

2.4.2. Synthesis of compound NFBDT-F

Under the protection of argon, DCHOBDT (0.10 g, 0.093 mmol) and INCN-F (0.07 g, 0.33 mmol) was dissolved in a dry CHCl₃ (50 mL) solution, and then pyridine (0.5 mL) was added to the mixture. After stirring at room temperature for 12 h, the mixture was poured into water and then extracted with CHCl₃ (30 mL × 2), the organic layer was dried over anhydrous Na₂SO₄ for 0.5 h. After removal of solvent, the crude product was purified by silica gel using petroleum ether/

CHCl_3 (1:2) as eluent and recrystallized from CHCl_3 and hexane to give NFBDT-F as a dark blue solid (0.102 g, 75.0% yield). Melting point: 235–239 °C. IR (KBr pellet): ν/cm^{-1} 2926.63, 2854.98, 2218.06, 1698.22, 1585.48, 1539.26, 1482.11, 1400.85, 1311.27, 1286.83, 1252.76, 1173.18, 1140.44, 1127.16, 988.99, 878.25, 739.75. ^1H NMR (400 MHz, CDCl_3): δ 8.86 (s, 2H), 8.70–8.67 (m, 0.5H), 8.35 (d, $J = 9.0$ Hz, 1.5H), 8.02 (s, 2H), 7.92–7.89 (m, 1.5H), 7.70 (s, 2H), 7.55–7.53 (m, 0.5H), 7.42–7.38 (m, 2H), 7.17 (d, $J = 8.2$ Hz, 8H), 7.09 (d, $J = 8.2$ Hz, 8H), 2.56 (t, $J = 7.7$ Hz, 8H), 1.59–1.56 (m, 8H), 1.30–1.25 (m, 24H), 0.87–0.84 (m, 12H). ^{13}C NMR (100 MHz, CDCl_3): δ 187.05, 165.42, 163.04, 158.79, 156.43, 156.38, 156.09, 144.14, 142.73, 142.31, 142.21, 140.62, 140.57, 138.89, 138.83, 138.49, 138.39, 138.26, 137.24, 133.03, 131.81, 128.98, 128.87, 128.04, 125.87, 125.77, 121.80, 121.57, 121.46, 121.39, 118.31, 114.47, 114.32, 112.96, 112.70, 69.50, 62.81, 35.61, 31.73, 31.31, 29.76, 29.72, 29.16, 22.76, 22.64, 14.16, 14.10. ^{19}F NMR (564 MHz, CDCl_3): δ –98.96 (s, 0.75F), –100.28 (s, 0.25F). HR-MS (MALDI): Found: [M + H]⁺ 1463.5208; molecular formula $\text{C}_{94}\text{H}_{80}\text{F}_2\text{N}_4\text{O}_2\text{S}_4$ requires [M + H]⁺, 1463.5210.

3. Results and discussion

3.1. Synthesis and characterization

The dialdehyde DCHOFTBDT was prepared by the Vilsmeier-Haack reaction as a white-yellow solid according to our previous work [47]. Both end group INCN-Me and INCN-F have two isomers, which cannot be separated due to their rather similar chemical structures. The mole ratio of the two isomers (5-isomer and 6-isomer) for INCN-F is 1:3 according to the ^1H NMR spectra in the Supporting Information, and 1:1.27 for INCN-Me. The desired product NFBDT-Me was then obtained via Knoevenagel condensation of the compound DCHOFTBDT with INCN-Me. NFBDT-F was synthesized by the similar procedure using fluorine substituted INCN. Owing to the isomerism of the two end groups, the two final products are all mixtures comprised of three isomers which cannot be separated at this stage. The two new isomeric mixtures were fully characterized by ^1H and ^{13}C NMR, and matrix assisted laser desorption ionization time of flight mass spectrometry (MALDI-TOF MS). These two molecules exhibit good solubility in common solvents such as chloroform and chlorobenzene. The thermal stability of these two molecules was investigated using thermogravimetric analysis (TGA) (Fig. 1a). The TGA curves of two compounds show that each of them exhibits excellent thermal stability with decomposition temperatures (T_d) over 350 °C.

Theoretical calculation (Fig. 2), based on density functional theory (DFT) at the B3LYP/6-31G (d) level, was performed. Frequency analysis was followed to ensure that the optimized geometries were at stable states, and the hexyl groups were replaced by methyl ones for simplification. Due to the different substituted position of the Me or F group at the end group, NFBDT-Me and NFBDT-F each also have 3 isomers, namely 6, 6-isomer, 5, 6-isomer and 5, 5-isomer. All of them were calculated and the structure and energy level are similar (Figs. S1 and S2). The results show that both molecules exhibit good coplanar conformations. Like other nonfullerene acceptors, the electron cloud density of HOMO is mainly localized at the central fused donor core part, while LUMO, the electron cloud prefers the end groups.

3.2. Optical absorption and electrochemical properties

The UV-Vis absorption spectra of these acceptors in CHCl_3 solution and as thin film are shown in Fig. 1c and d, and the corresponding data are summarized in Table 1. Both of these two acceptors exhibit strong and broad absorption in the region of 550–750 nm. In solutions, compared to the non-substituted molecule NFBDT, NFBDT-Me displays a rather similar absorption, while NFBDT-F displays a red-shift of ~14 nm at maximum absorption peak (λ_{max}). The maximum molar

extinction coefficients are determined to be 2.05×10^5 and $2.17 \times 10^5 \text{ M}^{-1} \text{ cm}^{-1}$, respectively, which are higher than NFBDT ($1.9 \times 10^5 \text{ M}^{-1} \text{ cm}^{-1}$). In the film, these two new molecules exhibit a clear red-shift compared to their maximum absorption peak in solution, with the λ_{max} at 725 and 743 nm, respectively. The optical band gap (E_g^{opt}) of NFBDT-Me estimated from the onset of their film absorption is 1.58 eV, which is larger than NFBDT, while the optical band gap of NFBDT-F (1.50 eV) is smaller than NFBDT.

The molecular energy levels were measured by electrochemical cyclic voltammetry (CV) under identical conditions to NFBDT. The highest occupied molecular orbital (HOMO) and lowest unoccupied molecular orbital (LUMO) energy levels are calculated from the onset oxidation and reduction potential, respectively. The HOMO and LUMO energy levels are –5.40 and –3.78 eV for NFBDT-Me, and –5.43 and –3.88 eV for NFBDT-F, respectively (Fig. 1b). The electrochemical and calculation data are listed in Table 1. The variation trends in the molecular energy levels are consistent with the results acquired from theoretical calculations. We can see that with the introduction of methyl on the end-capping group, the LUMO level up-lifts a little while the HOMO level remains the same. This indicates that a higher V_{oc} could be obtained in non-fullerene OSCs. For NFBDT-F, both HOMO and LUMO decrease a little due to the effect of the electron-withdrawing fluorine on the end-capping group.

3.3. Photovoltaic performance

Solution-processed BHJ devices were fabricated using these small molecules as the electron acceptor with a normal device structure of ITO/PEDOT:PSS (poly(3,4-ethylenedioxythiopene):poly(styrenesulfonate))/PBDB-T: Acceptor/PDIN (N,N' -bis(propylenedimethylamine)-3,4:9,10-perylene diimide)/Al. Taking the UV-Vis absorption spectra into consideration, we selected PBDB-T as donor material to fabricate their BHJ devices. The optimal D/A weight ratio is 1:0.6 for PBDB-T:NFBDT-Me, and 1:1 for PBDB-T:NFBDT-F. OSC devices based on the as-cast PBDB-T:NFBDT-Me films showed PCEs of 8.68%, while after chloroform solvent vapor annealing treatment (SVA), the PCE increased to 11.00%. For PBDB-T:NFBDT-F films, the PCE increased from 8.58% to 10.62% with SVA. Benefiting from the higher LUMO level, the devices based on NFBDT-Me obtained a high V_{oc} of 0.909 V. Due to the more red-shifted absorption, the devices based on NFBDT-F had a higher J_{sc} of 19.28 mA cm^{-2} compared with NFBDT-Me and NFBDT. The current-density–voltage (J – V) curves of the OSCs based on PBDB-T:NFBDT-Me/NFBDT-F with the optimal photovoltaic performance are summarized in Fig. 3a, and the corresponding photovoltaic parameters are listed in Table 2.

Their external quantum efficiency (EQE) curves of the best devices were measured as shown in Fig. 3b, where the devices with NFBDT-Me and NFBDT-F exhibit photo-to-current responses from 300 to 800 nm. It is obvious that the device based on NFBDT-F shows much higher EQE than NFBDT-Me at the wavelength from 600 to 800 nm. The NFBDT-F based device has the widest spectral response range of these three acceptors. The EQE of NFBDT-F is higher than that of NFBDT, while the EQE of NFBDT-Me is lower. The calculated J_{sc} obtained from the EQE curves are 16.70 and 18.58 mA cm^{-2} , respectively, which show a good match with the J_{sc} values obtained from the J – V curves.

The active layer morphologies were measured by atomic force microscopy (AFM) and transmission electron microscopy (TEM). As shown in the AFM images (Fig. 4a–c), the three SVA-treated blend films of PBDB-T:NFBDT, PBDB-T: NFBDT-Me, PBDB-T: NFBDT-F all showed low root-mean-square roughness with values of 1.44, 1.77 and 2.57 nm, respectively, indicating good film quality. Furthermore, the TEM images (Fig. 4d–f) indicate that all the three films formed evident interpenetrating network, which are consistent with the AFM images and their good device performances. From the AFM images and the TEM images, no obvious phase separation or excessive aggregation can be found for the NFBDT-Me and NFBDT-F based films, which is the same as for NFBDT. This kind of morphology is of benefit for the exciton

dissociation efficiency and charge transport in the OSC devices.

The mobilities of the optimized devices were measured by the space charge limited current (SCLC) method. The hole and electron mobilities for NFBDT-Me based devices are 2.07×10^{-4} and $1.68 \times 10^{-4} \text{ cm}^2 \text{ V}^{-1} \text{ s}^{-1}$, respectively. For NFBDT-F based devices, the hole and electron mobilities are 2.49×10^{-4} and $1.33 \times 10^{-4} \text{ cm}^2 \text{ V}^{-1} \text{ s}^{-1}$, respectively. Their hole and electron mobilities are of the same order of magnitudes to those of NFBDT. While each of them exhibited slightly more balanced electron and hole mobilities than PBDB-T: NFBDT based films, and this might have contribution to the higher FF for corresponding devices.

4. Conclusion

We have designed and synthesized two new small-molecule non-fullerene acceptors named NFBDT-Me and NFBDT-F, respectively. The devices based on NFBDT-Me exhibited a PCE of 11.00% due to the enhanced V_{oc} of 0.909 V, and the devices based on NFBDT-F demonstrated a PCE of 10.62% attributed to the increase of J_{sc} . Both of them are improved compared to that of NFBDT (10.42%). The result demonstrated that changing different substitutions on the end-capping group could finely tune the energy levels for better photovoltaic performance. We believe that higher PCE would be achieved through much more delicate molecule design and device optimizations.

Acknowledgments

The authors gratefully acknowledge the financial support from MOST (Grant Nos. 2014CB643502) and NSFC (Grant Nos. 51773095, 91633301) of China and Tianjin city (Grant Nos. 17JCJQJC44500, 17JCZDJC31100), 111 Project (Grant Nos. B12015).

Appendix A. Supplementary data

Supplementary data related to this article can be found at <http://dx.doi.org/10.1016/j.dyepig.2018.03.061>.

References

- [1] Yu G, Gao J, Hummelen JC, Wudl F, Heeger AJ. Polymer photovoltaic cells: enhanced efficiencies via a network of internal donor-acceptor heterojunctions. *Science* 1995;270(5243):1789–91.
- [2] Krebs FC. Fabrication and processing of polymer solar cells: a review of printing and coating techniques. *Sol Energy Mat Sol C* 2009;93(4):394–412.
- [3] Li G, Zhu R, Yang Y. Polymer solar cells. *Nat Photonics* 2012;6(3):153–61.
- [4] Liu C, Yi C, Wang K, Yang Y, Bhattacharyya RS, Tsige M, et al. Single-junction polymer solar cells with over 10% efficiency by a novel two-dimensional donor-acceptor conjugated copolymer. *ACS Appl Mater Interfaces* 2015;7(8):4928–35.
- [5] Chen JD, Cui C, Li YQ, Zhou L, Ou QD, Li C, et al. Single-junction polymer solar cells exceeding 10% power conversion efficiency. *Adv Mater* 2015;27(6):1035–41.
- [6] Kan B, Li M, Zhang Q, Liu F, Wan X, Wang Y, et al. A series of simple oligomer-like small molecules based on oligothiophenes for solution-processed solar cells with high efficiency. *J Am Chem Soc* 2015;137(11):3886–93.
- [7] Liu Y, Zhao J, Li Z, Mu C, Ma W, Hu H, et al. Aggregation and morphology control enables multiple cases of high-efficiency polymer solar cells. *Nat Commun* 2014;5:5293.
- [8] He Z, Xiao B, Liu F, Wu H, Yang Y, Xiao S, et al. Single-junction polymer solar cells with high efficiency and photovoltage. *Nat Photonics* 2015;9(3):174–9.
- [9] Zhang SQ, Ye L, Zhao WC, Yang B, Wang Q, Hou JH. Realizing over 10% efficiency in polymer solar cell by device optimization. *Sci China Chem* 2015;58(2):248–56.
- [10] Zhao W, Li S, Yao H, Zhang S, Zhang Y, Yang B, et al. Molecular optimization enables over 13% efficiency in organic solar cells. *J Am Chem Soc* 2017;139(21):7148–51.
- [11] Li S, Ye L, Zhao W, Zhang S, Mukherjee S, Ade H, et al. Energy-level modulation of small-molecule electron acceptors to achieve over 12% efficiency in polymer solar cells. *Adv Mater* 2016;28(42):9423–9.
- [12] Zhao F, Dai S, Wu Y, Zhang Q, Wang J, Jiang L, et al. Single-junction binary-blend nonfullerene polymer solar cells with 12.1% efficiency. *Adv Mater* 2017;29(18):1700144.
- [13] Zhao JB, Li YK, Yang GF, Jiang K, Lin HR, Ade H, et al. Efficient organic solar cells processed from hydrocarbon solvents. *Nat Energy* 2016;1:15027.
- [14] Zhao W, Li S, Zhang S, Liu X, Hou J. Ternary polymer solar cells based on two acceptors and one donor for achieving 12.2% efficiency. *Adv Mater* 2017;29(2):1604059.
- [15] Xiao Z, Jia X, Li D, Wang S, Geng X, Liu F, et al. 26 mA cm⁻² J(sc) from organic solar cells with a low-bandgap nonfullerene acceptor. *Sci Bull* 2017;62(22):1494–6.
- [16] Koster LJA, Mihailatchi VF, Blom PWM. Ultimate efficiency of polymer/fullerene bulk heterojunction solar cells. *Appl Phys Lett* 2006;88(9):093511.
- [17] Qiu N, Zhang H, Wan X, Li C, Ke X, Feng H, et al. A new nonfullerene electron acceptor with a ladder type backbone for high-performance organic solar cells. *Adv Mater* 2017;29(6):1604964.
- [18] Wu Q, Zhao D, Schneider AM, Chen W, Yu L. Covalently bound clusters of alpha-substituted PDI-rival electron acceptors to fullerene for organic solar cells. *J Am Chem Soc* 2016;138(23):7248–51.
- [19] Dai S, Zhao F, Zhang Q, Lau TK, Li T, Liu K, et al. Fused nonacyclic electron acceptors for efficient polymer solar cells. *J Am Chem Soc* 2017;139(3):1336–43.
- [20] Liu F, Zhou Z, Zhang C, Vergote T, Fan H, Liu F, et al. A thieno[3,4-b]thiophene-based nonfullerene electron acceptor for high-performance bulk-heterojunction organic solar cells. *J Am Chem Soc* 2016;138(48):15523–6.
- [21] Cao QF, Xiong WT, Chen HJ, Cai GS, Wang G, Zheng LP, et al. Design, synthesis, and structural characterization of the first dithienocyclopentacarbazole-based n-type organic semiconductor and its application in non-fullerene polymer solar cells. *J Mater Chem A* 2017;5(16):7451–61.
- [22] Liu Y, Zhang Z, Feng S, Li M, Wu L, Hou R, et al. Exploiting noncovalently conformational locking as a design strategy for high performance fused-ring electron acceptor used in polymer solar cells. *J Am Chem Soc* 2017;139(9):3356–9.
- [23] Zhao J, Li Y, Lin H, Liu Y, Jiang K, Mu C, et al. High-efficiency nonfullerene organic solar cells enabled by a difluorobenzothiadiazole-based donor polymer combined with a properly matched small molecule acceptor. *Energy Environ Sci* 2015;8(2):520–5.
- [24] Yang Y, Zhang ZG, Bin H, Chen S, Gao L, Xue L, et al. Side-Chain isomerization on an n-type organic semiconductor ITIC acceptor makes 11.77% high efficiency polymer solar cells. *J Am Chem Soc* 2016;138(45):15011–8.
- [25] Li S, Liu W, Li C-Z, Lau T-K, Lu X, Shi M, et al. A nonfullerene acceptor with a fully fused backbone for efficient polymer solar cells with a high open-circuit voltage. *J Mater Chem A* 2016;4(39):14983–7.
- [26] Zuo L, Yu J, Shi X, Lin F, Tang W, Jen AK. High-efficiency nonfullerene organic solar cells with a parallel tandem configuration. *Adv Mater* 2017;29(34):1702547.
- [27] Lin Y, He Q, Zhao F, Huo L, Mai J, Lu X, et al. A facile planar fused-ring electron acceptor for as-cast polymer solar cells with 8.71% efficiency. *J Am Chem Soc* 2016;138(9):2973–6.
- [28] Lin Y, Wang J, Zhang ZG, Bai H, Li Y, Zhu D, et al. An electron acceptor challenging fullerenes for efficient polymer solar cells. *Adv Mater* 2015;27(7):1170–4.
- [29] Lin Y, Zhao F, He Q, Huo L, Wu Y, Parker TC, et al. High-performance electron acceptor with thiienyl side chains for organic photovoltaics. *J Am Chem Soc* 2016;138(14):4955–61.
- [30] Xiao Z, Jia X, Ding L. Ternary organic solar cells offer 14% power conversion efficiency. *Sci Bull* 2017;62(23):1562–4.
- [31] Hwang YJ, Courtright BA, Ferreira AS, Tolbert SH, Jenekhe SA. 7.7% efficient all-polymer solar cells. *Adv Mater* 2015;27(31):4578–84.
- [32] Jung JW, Jo JW, Chueh CC, Liu F, Jo WH, Russell TP, et al. Fluoro-substituted n-type conjugated polymers for additive-free all-polymer bulk heterojunction solar cells with high power conversion efficiency of 6.71%. *Adv Mater* 2015;27(21):3310–7.
- [33] Liu Y, Mu C, Jiang K, Zhao J, Li Y, Zhang L, et al. A tetraphenylethylene core-based 3D structure small molecular acceptor enabling efficient nonfullerene organic solar cells. *Adv Mater* 2015;27(6):1015–20.
- [34] Zhou Y, Kurosawa T, Ma W, Guo Y, Fang L, Vandewal K, et al. High performance all-polymer solar cell via polymer side-chain engineering. *Adv Mater* 2014;26(22):3767–72.
- [35] Wang JL, Wu Z, Miao JS, Liu KK, Chang ZF, Zhang RB, et al. Solution-processed diketopyrrolopyrrole-containing small-molecule organic solar cells with 7.0% efficiency: in-depth investigation on the effects of structure modification and solvent vapor annealing. *Chem Mater* 2015;27(12):4338–48.
- [36] Li S, Liu W, Shi M, Mai J, Lau T-K, Wan J, et al. A spirobifluorene and diketopyrrolopyrrole moieties based nonfullerene acceptor for efficient and thermally stable polymer solar cells with high open-circuit voltage. *Energ Environ Sci* 2016;9(2):604–10.
- [37] Josse P, Dalinot C, Jiang Y, Dabos-Seignon S, Roncali J, Blanchard P, et al. Phthalimide end-capped thienoisindigo and diketopyrrolopyrrole as nonfullerene molecular acceptors for organic solar cells. *J Mater Chem A* 2016;4(1):250–6.
- [38] Li MM, Liu YT, Ni W, Liu F, Feng HR, Zhang YM, et al. A simple small molecule as an acceptor for fullerene-free organic solar cells with efficiency near 8%. *J Mater Chem A* 2016;4(27):10409–13.
- [39] Gao K, Li LS, Lai TQ, Xiao LG, Huang Y, Huang F, et al. Deep absorbing porphyrin small molecule for high-performance organic solar cells with very low energy losses. *J Am Chem Soc* 2015;137(23):7282–5.
- [40] Hwang YJ, Earmme L, Courtright BA, Eberle FN, Jenekhe SA. n-Type semiconducting naphthalene diimide-perylene diimide copolymers: controlling crystallinity, blend morphology, and compatibility toward high-performance all-polymer solar cells. *J Am Chem Soc* 2015;137(13):4424–34.
- [41] Zhong Y, Trinh MT, Chen R, Wang W, Khlyabich PP, Kumar B, et al. Efficient organic solar cells with helical perylene diimide electron acceptors. *J Am Chem Soc* 2014;136(43):15215–21.
- [42] Holliday S, Ashraf RS, Wadsworth A, Baran D, Yousaf SA, Nielsen CB, et al. High-efficiency and air-stable P3HT-based polymer solar cells with a new nonfullerene acceptor. *Nat Commun* 2016;7:11585.
- [43] Yao H, Cui Y, Yu R, Gao B, Zhang H, Hou J. Design, synthesis, and photovoltaic characterization of a small molecular acceptor with an ultra-narrow band gap. *Angew Chem Int Ed Engl*. 2017;56(11):3045–9.

- [44] Li T, Dai S, Ke Z, Yang L, Wang J, Yan C, et al. Fused tris(thienothiophene)-based electron acceptor with strong near-infrared absorption for high-performance as-cast solar cells. *Adv Mater* 2018;30(10):1705969.
- [45] Kawashima K, Fukuhara T, Suda Y, Suzuki Y, Koganezawa T, Yoshida H, et al. Implication of fluorine atom on electronic properties, ordering structures, and photovoltaic performance in naphthobisthiadiazole-based semiconducting polymers. *J Am Chem Soc* 2016;138(32):10265–75.
- [46] Zhang M, Guo X, Zhang S, Hou J. Synergistic effect of fluorination on molecular energy level modulation in highly efficient photovoltaic polymers. *Adv Mater* 2014;26(7):1118–23.
- [47] Kan B, Feng H, Wan X, Liu F, Ke X, Wang Y, et al. Small-molecule acceptor based on the heptacyclic benzodi(cyclopentadithiophene) unit for highly efficient nonfullerene organic solar cells. *J Am Chem Soc* 2017;139(13):4929–34.
- [48] Wang J, Wang W, Wang X, Wu Y, Zhang Q, Yan C, et al. Enhancing performance of nonfullerene acceptors via side-chain conjugation strategy. *Adv Mater* 2017;29(35):1702125.
- [49] Chen YL, Chang CY, Cheng YJ, Hsu CS. Synthesis of a new ladder-type benzodi(cyclopentadithiophene) arene with forced planarization leading to an enhanced efficiency of organic photovoltaics. *Chem Mater* 2012;24(20):3964–71.
- [50] Frisch M, Trucks G, Schlegel H, Scuseria G, Robb M, Cheeseman J, Scalmani G, Barone V, Mennucci B, Petersson G, Nakatsuji H, Caricato M, Li X, Hratchian H, Izmaylov A, Bloino J, Zheng G, Sonnenberg J, Hada M, Ehara M, Toyota K, Fukuda R, Hasegawa J, Ishida M, Nakajima T, Honda Y, Kitao O, Nakai H, Vreven T, Montgomery Jr. J, Peralta J, Ogliaro F, Bearpark M, Heyd J, Brothers E, Kudin K, Staroverov V, Keith T, Kobayashi R, Normand J, Raghavachari K, Rendell A, Burant J, Iyengar S, Tomasi J, Cossi M, Rega N, Millam J, Klene M, Knox J, Cross J, Bakken V, Adamo C, Jaramillo J, Gomperts R, Stratmann R, Yazeyev O, Austin A, Cammi R, Pomelli C, Ochterski J, Martin R, Morokuma K, Zakrzewski V, Voth G, Salvador P, Dannenberg J, Dapprich S, Daniels A, Farkas O, Foresman J, Ortiz J, Cioslowski J, Fox D. Gaussian 09, Revision B.01. Wallingford CT: Gaussian, Inc.; 2010.